

UNIFYING THE ZOO OF JET-DRIVEN STELLAR EXPLOSIONS

DAVIDE LAZZATI¹, BRIAN J. MORSONY², CHRISTOPHER H. BLACKWELL^{1,3}, MITCHELL C. BEGELMAN^{4,5}

Draft version March 14, 2012

ABSTRACT

We present a set of numerical simulations of stellar explosions induced by relativistic jets emanating from a central engine sitting at the center of compact, dying stars. We explore a wide range of durations of the central engine activity, two candidate stellar progenitors, and two possible values of the total energy release. We find that even if the jets are narrowly collimated, their interaction with the star unbinds the stellar material, producing a stellar explosion. We also find that the outcome of the explosion can be very different depending on the duration of the engine activity. Only the longest-lasting engines result in successful gamma-ray bursts. Engines that power jets only for a short time result in relativistic supernova explosions, akin to observed engine-driven SNe such as SN2009bb. Engines with intermediate durations produce weak gamma-ray bursts, with properties similar to nearby bursts such as GRB 980425. Finally, we find that the engines with the shortest durations, if they exist in nature, produce stellar explosions that lack sizable amounts of relativistic ejecta and are therefore dynamically indistinguishable from ordinary core-collapse supernovae.

Subject headings: Gamma-ray burst: general — Hydrodynamics — supernovae: general — supernovae: individual (SN2009bb)

1. INTRODUCTION

Massive stars end their life with powerful explosions called supernovae (SNe, Woosley & Weaver 1986). Some SNe are brighter than others, and in extreme cases a gamma-ray burst (GRB) - the brightest explosion in the present universe - is produced (Hjorth et al. 2003; Stanek et al. 2003; Woosley & Bloom 2006). It is believed that a GRB is associated with a SN when the progenitor star is compact, its stellar core has fast rotation, and the collapse of the core creates a fast spinning compact object that releases bipolar jets of relativistic matter and energy (MacFadyen & Woosley 1999; Woosley & Heger 2006). Recent observations (Soderberg et al. 2010; Bietenholz et al. 2010) and theoretical work (Khokhlov et al. 1999; Burrows et al. 2007; Wheeler & Akiyama 2010; Nakamura et al. 2012) have shown that an engine of the same kind may be present in some more mundane SNe that differ from their normal counterparts only by the presence of a fast and bright radio transient.

Long-duration GRBs are powered by light, highly relativistic jets produced by a still mysterious compact object sitting at the center of an exploding massive star. The first hurdle that the newly born jet has to overcome to become a GRB is the crossing of its progenitor star. The light, relativistic plasma has to bore a hole through the cold, dense stellar material without being excessively polluted by the star's baryons that would slow it down and prevent the release of the high-frequency photons that characterize the GRB prompt emission (Piran 1999, Kaneko et al. 2006). Numerical simulations showed that the jet forms a bow shock in the stellar material that advances at sub-relativistic speed, shedding some of

its energy in the process (MacFadyen & Woosley 1999; Aloy et al. 2000; Zhang et al. 2003, 2004; Morsony et al. 2007; Mizuta & Aloy 2009). The “wasted” energy is accumulated in a hot cocoon that drives shock waves into the star (Ramirez-Ruiz et al. 2002; Lazzati & Begelman 2005; Bromberg et al. 2011b), unbinding it and possibly producing the supernova associated with the burst (Hjorth et al. 2003; Stanek et al. 2003). The time it takes a typical GRB jet to cross the star and break out on the surface is approximately ten seconds (Morsony et al. 2007). However, the duration distribution of GRBs includes bursts as short as two seconds, requiring the existence of engines with a duration barely long enough to power the jet until the breakout time (Kouveliotou et al. 1983). Engines with even shorter activity could exist in nature. However, their detection is challenging since they do not produce a clear electromagnetic signature such as a GRB.

Observations of weak GRBs such as GRB 980425 associated with SN1998bw (Galama et al. 1998; Kulkarni et al. 1998), X-ray flares such as XRF080109 (Mazzali et al. 2008; Soderberg et al. 2008), and relativistic radio bright supernovae (SN) such as SN2009bb (Soderberg et al. 2010; Bietenholz et al. 2010) call for diversity in the properties of the engines and/or the progenitors that power the explosion. In this paper we investigate the role of the duration of the engine activity on the explosive outcome of compact stars with a GRB-like central engine. Keeping all the jet and progenitor properties fairly constant, we vary the engine duration, exploring the consequences of the non-linearity of the jet propagation velocity for increasing engine luminosities. The paper is organized as follows. In Section 2 we present our numerical simulations, in Section 3 we describe our results, in Section 4 we outline an analytical model to interpret our results, and in Section 5 we discuss the implications and limitations of our study.

2. NUMERICAL SIMULATIONS

All the simulations presented in this paper were performed with the FLASH code (Fryxell et al. 2000). We adopted a minimum resolution of 4×10^6 cm at the highest level of refinement. At this resolution the transverse dimension of the

¹ Department of Physics, NC State University, 2401 Stinson Drive, Raleigh, NC 27695-8202

² Department of Astronomy, University of Wisconsin-Madison, 2535 Sterling Hall, 475 N. Charter Street, Madison WI 53706-1582

³ Department of Physics, Optics Building, University of Alabama in Huntsville, Huntsville, AL 35899, USA

⁴ JILA, University of Colorado, 440 UCB, Boulder, CO 80309-0440

⁵ University of Colorado, Department of Astrophysical and Planetary Sciences, 389 UCB, Boulder, CO 80309-0389

injected jet is resolved into 44 elements. This resolution was chosen after verifying that simulations performed at twice the resolution would yield consistent results (Figure 1). Our simulations do not include magnetic fields, due to the technical challenge of performing MHD calculations with relativistic motions on an adaptive mesh. Our simulations do not consider nuclear burning since its inclusion would have made the simulations too long to perform at the adequate resolution. As a consequence, ejection velocities are marginally affected. Finally, gravity from a central mass and self-gravity are neglected since the characteristic time-scales of the jet-star interaction are much shorter than the dynamical time of the progenitor star's collapse. Due to the absence of gravity, our progenitor star expands by a modest 2% of its original size in the 100 seconds of the simulations. The dynamical time scale at the stellar surface is $\tau_{\text{dyn}} \simeq 10^5$ s, while at our inner boundary it is $\tau_{\text{dyn}} \simeq 10$ s, comparable to the break-out time of our jets. All our simulations adopted realistic GRB stellar progenitors: models 16TI and 12OM from Woosley & Heger (2006). Model 16TI is a 16 solar-mass Wolf-Rayet star with an initial metallicity 1% solar and angular momentum $L = 3.3 \times 10^{52}$ erg s. The mass of the star at pre-explosion is 13.95 solar masses and its radius is 4.1×10^{10} cm, corresponding to 0.6 solar radii. Model 12OM is a 12 solar-mass Wolf-Rayet star with an initial metallicity 10% solar and angular momentum $L = 2.5 \times 10^{52}$ erg/s. The mass of the star at pre-explosion is 9.5 solar masses and its radius is 4.8×10^{10} cm, corresponding to 0.7 solar radii.

In all cases, a relativistic jet with opening angle $\theta_0 = 10^\circ$ was injected as a boundary condition at a distance $r_0 = 10^9$ cm from the stellar center. The engine luminosity varied among simulations depending on the duration of the engine activity in order to keep the total energy budget fixed to $E = 3 \times 10^{51}$ erg (one set of simulations for the 16TI and 12OM progenitor models) or $E = 10^{52}$ erg (one set of simulations for the 16TI progenitor). In each simulation, the engine luminosity was kept constant until the cutoff time, when the engine was abruptly turned off. All jets were injected with Lorentz factor $\Gamma_0 = 5$ and with enough internal energy to reach an asymptotical $\Gamma_\infty = 400$ upon complete, non-dissipational acceleration. This jet configuration was used numerous times to reproduce the properties of successful GRBs (Morsony et al. 2007, 2010; Lazzati et al. 2009, 2011). A false color still of the density and expansion velocity of one of our simulations is shown in Figure 2.

3. RESULTS

The simulations were analyzed for the jet dynamics, the presence of an associated stellar explosion, and the nature of the ensuing explosion. All our simulations resulted in the explosion of the progenitor star. However, the fraction of the mass that was ejected into the interstellar medium varied with the engine activity time. The shorter t_{eng} was, the higher the fraction of the star mass that achieved escape velocity. Analyzing the frames at 15 s after the engine onset for our simulations of a the 16TI progenitor with $E = 3 \times 10^{51}$ erg, we found that 95% of the progenitor mass had been ejected by our shortest-duration engine ($t_{\text{eng}} = 3.0$ s), while 88% of the progenitor mass had been ejected by our longest engine ($t_{\text{eng}} = 15.0$ s). We also found that the stellar explosions are not directly due to the jet, which occupies only a small fraction of the solid angle, similar to results obtained for non-relativistic jets (Khokhlov et al. 1999). The jet propagation,

however, produces a hot, high-pressure cocoon that drives a conical shock into the stellar material. For that reason, the star does not explode spherically. At the time of the jet breakout, the star-exploding shock reaches the pole of the star but is still less than halfway through along the equator. For example, the equatorial breakout took three times longer than the polar one in our $t_{\text{eng}} = 6.0$ s simulation. Computing the fraction of ejected mass from a simulation that does not include gravity is non-trivial and, to some extent, not rigorous. At any given time in the simulation we proceeded as follows to evaluate whether a parcel of matter located at radius r is bound or not. We first computed the amount of mass inside a sphere of radius r and evaluated the escape velocity from such a mass distribution. Subsequently, we compared the escape velocity with the radial component of the velocity of the parcel of matter. If the parcel velocity is larger than the escape velocity we label the matter as unbound, otherwise we consider it still bound, eventually falling back to the stellar remnant. This procedure has two limitations. First the mass distribution is not spherically symmetric and therefore the simple approximation that the gravity on a point mass only depends on the mass in the inside sphere is not correct. Second, the lack of gravity in the simulation affects the mass velocity itself. As a consequence, the values of the unbound mass fraction reported above should be considered as indicative.

The difference in the explosive outcome is due to the non-linearity in the jet propagation. If the propagation velocity of the jet head would scale linearly with the engine luminosity, explosions with the same energy budget would look alike since the jet would either stall inside the star or breakout, independently of the engine luminosity and duration. However, we find that the jet head propagates at a speed that scales less than linearly with the luminosity (Figure 3, Section 4). The non-linearity is brought about by the feedback between the jet and the high-pressure cocoon that surrounds it. A more luminous jet has higher internal pressure that makes its head wider and therefore its propagation harder, shocking a larger fraction of the stellar material. This, in turn, makes the cocoon more energetic and the higher cocoon pressure squeezes the jet head facilitating its propagation.

The different jet propagation velocities imply that in some configurations the jet breaks out the star's surface, while in others it does not. We find that there are three conditions that have relevance to the star's explosion outcome (Figure 4). If the engine activity time is short enough, the engine turns off while the jet head is still buried inside the star. As the engine turns off, the tail of the jet detaches from the engine and eventually catches up with the jet's head. If this happens while the jet head is inside the star, all the bulk relativistic motion is lost and the star's explosion is entirely driven by the high-pressure cocoon that is left, resulting in an ordinary-looking supernova with little energy in relativistic ejecta. This condition is shown with a dotted line in Figure 4. Alternatively, the engine may turn off while the jet head is inside the star but, by the time the tail of the jet has caught up with the head, the head has already broken free. In this case a small fraction of the material moving with bulk relativistic speed survives and, depending on the details, produces observable signals in the form of either a bright radio transient or a weak, GRB980425-like burst. This condition is shown in Figure 4 with a dashed line. Finally, if the engine active time is long enough, the jet breaks out while the engine is still active. In this case a fully developed GRB is expected. Figure 4 shows that all these conditions are realized by an engine with constant energy but

varying activity time. The comparison between three sets of simulations shows that the engine duration that characterizes each type of explosion depends also on the total energy budget and on the progenitor structure. The density and velocity maps of a simulation that produces the intermediate outcome (16 solar-mass progenitor, $E = 3 \times 10^{51}$ erg, $t_{\text{eng}} = 7.5$ s) are shown in Figure 2.

Figure 5 shows a quantitative comparison between the results of our simulations and the properties of type Ibc SNe and jet-driven stellar explosions as derived from observations of their associated radio transient (Soderberg et al. 2010). Non-thermal radio emission from SNe is produced by the interaction of the highest-velocity ejecta with the surrounding ambient medium (Chevalier 1998; Weiler et al. 2002; Chevalier & Fransson 2006). We selected the ejecta moving with $\beta > 0.7$ (where β is the velocity in unit of the speed of light) as the material contributing to the radio transient and we computed the expansion speed as the energy-weighted average of their velocity. Note that the computation was performed for β even though $\beta\Gamma$ is plotted in Figure 5. The analysis was performed in the last frame that we were able to compute, either at $t = 100$ s or at the time at which FLASH would run into a numerical instability (often occurring around the time of the shock breakout in the equatorial direction). The energy in relativistic ejecta is a fairly robust number, as long as it is computed after the jet/cocoon breakout along the polar direction. Figure 6 shows the evolution of the energy in the ejecta of one of our longest runs as a function of time after the engine onset. The time of the jet/cocoon breakout along the polar and equatorial directions are shown. We also checked that the value of the energy in relativistic ejecta has a very small dependence on whether the actual expansion velocity or the asymptotic one are considered (the asymptotic expansion velocity is the one attained once all the internal energy has been converted in bulk outward velocity). In all cases the energy once the asymptotic velocity is attained is larger by less than 10% with respect to the one shown in the figures. This is consistent with the fact that the energy in Figure 6 is constant. Should significant acceleration take place, a marked evolution in the energy would be observed. In Figure 7 we show instead the entire cumulative distribution of the energy of the ejecta for three representative cases. All the simulations shown are performed with the 16TI progenitor and have total energy $E = 3 \times 10^{51}$ erg.

4. JET PROPAGATION MODEL

The propagation speed of the head of the jet can be found by enforcing pressure balance along the discontinuity between the jet head and the progenitor star material. The pressure balance reads (Matzner 2003; Bromberg et al. 2011b):

$$\rho_j h_j \Gamma_j^2 (\beta_j - \beta_h)^2 + P_j = \rho_a h_a \Gamma_a^2 \beta_h^2 + P_a \quad (1)$$

where β , Γ , ρ , P , and $h = 1 + 4p/\rho c^2$ are the velocity in units of the speed of light, the Lorentz factor, the mass density, the pressure, and the dimensionless specific enthalpy, respectively. An adiabatic index $\hat{\gamma} = 4/3$ is used in the enthalpy expression. The subscript j refers to the jet material, the subscript h refers to the jet head, and the subscript a refers to the ambient medium, in our case the progenitor star. The above equation is greatly simplified in the case of a hot, light relativistic jet slowly advancing into a cold, high-density ambient medium. In that case, the pressure terms can be neglected and we can use the approximations $\Gamma_h = 1$, $\beta_h \ll \beta_j$, $\beta_j = 1$,

and $P_j \gg \rho_j c^2$. These simplifications yield: $\rho_j h_j \Gamma_j^2 = \rho_a h_a \beta_h^2$ which, solving for β_h and using the definition of h becomes:

$$\beta_h = \sqrt{\frac{4P_j}{\rho_a c^2}} \Gamma_j \quad (2)$$

Under the assumption that the pressure of the jet at the head is in equilibrium with the pressure of the cocoon that surrounds the jet, we have $P_j = P_c = E_c/3V_c$ where P_c , E_c , and V_c are the cocoon pressure, energy, and volume, respectively. Under our assumption of sub-relativistic speed of the jet head, the cocoon energy is given by the energy ejected by the central engine: $E_c = L_j t = L_j r_h / c \beta_h$, where L_j is the engine luminosity and r_h is the distance travelled by the jet head. The cocoon volume is given, assuming an ellipsoidal shape, by:

$$V_c = \frac{4\pi}{3} r_h r_\perp^2 = \frac{4\pi}{3} r_h (v_\perp t)^2 = \frac{4\pi}{3} \frac{P_c}{\rho_a} \frac{r_h^3}{c^2 \beta_h^2} \quad (3)$$

where r_\perp is the transverse size of the cocoon, v_\perp is the velocity of the shock driven by the cocoon into the stellar material, and we have used the Kompaneets approximation in the last step (Begelman & Cioffi 1989; Lazzati & Begelman 2005). Using Eq. 3 we find the cocoon pressure as:

$$P_c = \sqrt{\frac{c L_j \rho_a \beta_h}{4\pi r_h^2}} \quad (4)$$

Finally, we need to find a relation between the jet pressure and Lorentz factor. The jet pressure is $P_j = L_j / (4c \Sigma_j \Gamma_j^2)$, where Σ_j is the transverse cross section of the jet. In case of non-dissipational acceleration, the jet Lorentz factor scales linearly with its transverse size, and we obtain:

$$\Gamma_j = \left(\frac{L_j \Gamma_0^2}{4c \Sigma_0 P_j} \right)^{1/4} \quad (5)$$

where Σ_0 and Γ_0 are the initial transverse cross section and Lorentz factor of the jet, respectively. The system of equations 2, 4, and 5 can now be solved for the jet head propagation velocity:

$$\beta_h = \left(\frac{4\Gamma_0^4}{\pi^3 c^9 \rho_a^3 r_0^4 \theta_0^4} \right)^{1/7} \frac{L_j^{3/7}}{r_h^{2/7}} \quad (6)$$

where we have used the identity $\Sigma_0 = \pi r_0^2 \theta_0^2$, r_0 being the jet injection radius and θ_0 its initial opening angle. The head velocity from Eq. 6 is compared to the simulation with thick black lines (dashed and dotted) results in Figure 3. We find that Eq. 6 reproduces fairly well the dependence of the head velocity on the jet luminosity. However, it overpredicts the head velocity by a factor ~ 4 . This discrepancy is likely due to the approximation made in Eq. 5, where it was assumed that the jet accelerates without dissipation until it is shocked at the jet-star discontinuity. In fact, several recollimation shocks are evident in our simulations. Such shocks reduce the jet speed and, as a consequence, also the speed of the head (see Eq. 2).

An alternative solution can be found by considering the ram pressure of the inner part of the jet, which is in free expansion, against the shear layer at the contact between the jet and star materials (Morsony et al. 2007; Bromberg et al. 2011b). From the results in Table 1 of Bromberg et al. (2011b) one

can easily find:

$$\beta_h = \frac{L_j^{1/3}}{c \rho_a^{1/3} r_h^{2/3} \theta_0^{4/3}} \quad (7)$$

The dependence of the jet head velocity on the jet luminosity is shown in Figure 3 with thin black lines. The results of our simulation are not able to distinguish between the derivation presented here (Eq. 6) and the Bromberg et al. (2011b) result. In either case, the jet head velocity is overestimated by a factor ~ 4 while the dependence on the jet luminosity is qualitatively reproduced.

5. DISCUSSION AND CONCLUSIONS

We presented a set of simulations aimed at exploring the role of the duration of the engine activity in the explosive phenomenology of compact massive progenitor stars. Our simulations suggest that the diversity in explosive outcomes (GRBs, weak-GRBs, X-ray flashes, relativistic radio-bright SNe) is not necessarily reflected by an analogous diversity in progenitor and engine properties. As a matter of fact just one of our simulation sets, for a given progenitor structure and a given total energy, can give examples of the whole zoo of engine-driven explosions, as long as the engine activity can have a wide range of durations, as observed in the GRB T_{90} distribution (Kouveliotou et al. 1983).

Jet-driven explosions like the ones we explore, however, do not seem to be able to reproduce the properties of the ordinary type Ibc SNe in the lower left corner of Figure 5. This is expected, since stellar evolution models predict that only a small fraction of massive star have the properties required to harbor a GRB engine in their center (Woosley & Heger 2006; see, however, Papish & Soker 2001 for an alternative opinion). However our simulations do predict that if jet engines with short active times exist they produce stellar explosions. For example the $t_{\text{eng}} = 3.0, 4.0, \text{ and } 5.0$ s simulations for the 16 solar-mass progenitor and total energy $E = 3 \times 10^{51}$ erg resulted in 90% of the stellar material unbound. Such explosions would not be associated with fast, bright radio transients. A member of this new class of explosions may have been recently identified in SN2010jp (Smith et al. 2011). It must be noted, however, that the comparison of our simulations with observations in the lower left corner of Figure 5 is severely affected by the somewhat arbitrary choice of a lower limit $\beta \geq 0.7$ for the material to be included in the calculation of the “relativistic” ejecta. As shown in Figure 7 (blue line), the energy distribution of ordinary-looking jet-driven SNe is very steep and a change in the velocity threshold affects dramatically the amount of energy labeled as “relativistic”. In addition, the data from the simulations are extracted just a few tens of seconds after the engine onset, while the radio data used by Soderberg et al. (2010) were taken on a time scale of weeks after the burst trigger. In order to accurately compare the weakest radio transients in Figure 5 to our simulations, it is required to evolve the simulations much farther in time and space to directly compute the radio emission, a task that is not feasible at the required resolution with current instrumentation. Additional signatures, such as asphericity, nucleosynthesis patterns, absorption and emission lines profiles, and linear polarization need to be explored in order to confirm our results and find observable quantities that could allow us to distinguish between radio-quiet jet-driven explosions and core-collapse SNe.

Our simulations predict that engines with a long duration

always produce a successful burst, while only within a certain duration interval they produce events of the intermediate classes, such as relativistic Ibc SNe and weak GRBs or X-ray flashes. Our 16TI progenitor, for example, produces intermediate events for $6 \leq t_{\text{eng}} \leq 10$ s and $2 \leq t_{\text{eng}} \leq 4.5$ s for the low-energy and high-energy engines, respectively. If the distribution of engine durations were flat, our mode would predict a larger rate of successful GRB events compared to events of the intermediate class. Such prediction would be inconsistent to current estimates, estimating the current rate of intermediate events either comparable to that of successful events (Soderberg et al. 2010) or an order of magnitude larger (Soderberg et al. 2006). Such comparison led Bromberg et al. (2011a) to conclude that low-luminosity GRBs have a different origin from successful GRBs. However, the intrinsic engine duration distribution is not known, and it may well be that due to the high angular momentum that is required in the collapsar model to sustain prolonged accretion onto the central compact object (MacFadyen & Woosley 1999, Woosley & Heger 2006), the intrinsic distribution is skewed towards short durations, explaining the high rate of intermediate class events. Further observations and a better theoretical understanding of the powering of relativistic jets will help make this constraint more useful for future comparison. It should also be pointed out that the viewing angle does have an influence on the burst energetics and spectrum for a given progenitor-engine pair (e.g., Lazzati et al. 2011), adding to the diversity of the events.

Our simulations also predict a correlation between the engine duration and the energy observed as electromagnetic radiation. When trying to compare this prediction with observations, one should keep in mind that the engine duration is not equal to the duration of the prompt emission (the T_{90}) and that the energy in radiation is the “true energy”, not the isotropic equivalent one. It is particularly difficult to connect the engine duration to the T_{90} duration. In most cases of successful bursts one has $t_{\text{eng}} > T_{90}$, but the difference between the two quantities can be large. For example, Lazzati et al. (2010) find that the same engine observed from different viewing angles can give rise to GRBs with durations spanning from a tenth of a second up to 100 seconds (the duration of the engine in that particular simulation). Such a diversity of durations of the radiative phase for a given engine duration is due to the interaction of the jet with the progenitor star. Observers very close to the jet axis see an initially very bright phase, due to the hydrodynamic collimation of the energy along the jet axis. Observers at larger angles, however, do not see any emission at early times since the jet has been collimated to an opening angle smaller than the angle of the line of sight. On the other side of the duration distribution, short engines can produce relatively long bursts or flashes since the dynamics of the ejecta is very different between events dominated by the shock breakout (e.g. Campana et al. 2006; Nakar & Sari 2012) and events dominated by fully developed, highly relativistic outflows.

As a final remark, it should be noted that the simulations that we have presented here do not include all the complex physics of a stellar explosion. The most important limitations are likely the facts that magnetic fields are not considered, that the jet is injected at a somewhat large radius, that the simulations are performed in 2D, and that the engine/jet properties are not self-consistently derived from the progenitor properties. All these limitations are likely to affect the details of the jet propagation. For example, a well-known 2D instabil-

ity produces the wedge of high-density, slow-moving material that is visible ahead of the jet in Figure 2. Such a wedge disappears in 3D simulations (Zhang et al. 2004) and its appearance in 2D simulations has the effect of making the jet propagation slightly slower. The bottom line is that the precise numerical values of the engine durations that correspond to each class of explosions are not to be taken at face value. Future, more refined simulations will likely update those values and are required to further evaluate the role of the engine duration in explaining the zoo of jet-driven stellar explosions.

Resources supporting this work were provided by the NASA HEC program through NAS. The software used in this work was in part developed by the DOE-supported ASC / Alliance Center for Astrophysical Thermonuclear Flashes at the University of Chicago. This work was supported in part by NASA Astrophysics Theory Program grant NNX09AG02G (MCB), NSF grant AST-0907872 (MCB), and Fermi GI program grant NNX10AP55G (DL & CHB). BJM is supported by an NSF Astronomy and Astrophysics Postdoctoral Fellowship under award AST-1102796.

REFERENCES

- Aloy, M. A., Müller, E., Ibáñez, J. M., Martí, J. M. & MacFadyen, A. I. 2000, *ApJ*, 531, L119
- Begelman, M. C., & Cioffi, D. F. 1989, *ApJ*, 345, L21
- Bietenholz, M. F. et al. 2011, *ApJ*, 725, 4
- Bromberg, O., Nakar, E., & Piran, T. 2011a, *ApJ*, 739, L55
- Bromberg, O., Nakar, E., Piran, T., & Sari, R. 2011b, *ApJ*, 740, 100
- Burrows, A., Dessart, L., Livne, E., Ott, C. D., & Murphy, J. 2007, *ApJ*, 664, 416
- Campana, S. et al. 2006, *Nature*, 442, 1008
- Chevalier, R. A. 1998, *ApJ*, 499, 810
- Chevalier, R. A., & Fransson, C. 2006, *ApJ*, 651, 381
- Fryxell, B., et al. 2000, *ApJS*, 131, 273
- Galama, T. J., et al. 1998, *Nature*, 395, 670
- Hjorth, J., et al. 2003, *Nature*, 423, 847
- Kaneko, Y., et al. 2006, *ApJS*, 166, 298
- Khokhlov, A. M., Höflich, P. A., Oran, E. S., Wheeler, J. C., Wang, L., & Chtchelkanova, A. Yu. 1999, *ApJ*, 524, L107
- Kouveliotou, C. et al. 1983, *ApJ*, 413, L101
- Kulkarni, S. R., et al. 1998, *Nature*, 395, 663
- Lazzati, D., & Begelman, M. C. 2005, *ApJ*, 629, 903
- Lazzati, D., Morsony, B. J., & Begelman, M. C. 2009, *ApJ*, 700, L47
- Lazzati, D., Morsony, B. J., & Begelman, M. C. 2010, *ApJ*, 717, 239
- Lazzati, D., Morsony, B. J., & Begelman, M. C. 2011, *ApJ*, 732, 34
- MacFadyen, A. I., & Woosley, S. E. 1999, *ApJ*, 524, 262
- Matzner, C. 2003, *MNRAS*, 345, 575
- Mazzali, P. A., et al. 2008, *Science*, 321, 1185
- Morsony, B. J., Lazzati, D., & Begelman, M. C. 2007, *ApJ*, 665, 569
- Morsony, B. J., Lazzati, D., & Begelman, M. C. 2010, *ApJ*, 723, 267
- Nagakura, H., Suwa, Y., and Ioka, K. 2012, submitted to *ApJ* (arXiv:1104.5691v1)
- Nakar, E. & Sari, R. 2012, *ApJ*, 747, 88
- Papish, O., and Soker, N. 2011, *MNRAS*, 416, 1697
- Piran, T. 1999, *Phys. Rep.*, 314, 575
- Ramirez-Ruiz, E., Celotti, A., Rees, M. J. 2002, *MNRAS*, 337, 1349
- Smith, N., et al. 2011, submitted to *MNRAS* (arXiv:1108.2868v1)
- Soderberg, A. M., et al. 2006, *Nature*, 442, 1014
- Soderberg, A. M., et al. 2008, *Nature*, 453, 469
- Soderberg, A. M., et al. 2010, *Nature*, 463, 513
- Stanek, K. Z., et al. 2003, *ApJ*, 591, L17
- Weiler, K. W., Panagia, N., Montes, M. J., & Sramek, R. A. 2002, *ARA&A*, 40, 387
- Wheeler, J. C., & Akiyama, S. 2010, *New Astronomy Reviews*, 54, 183
- Woosley, S. E., & Weaver, T. A. 1986, *ARA&A*, 24, 205
- Woosley, S. E., & Bloom, J. S. 2006, *ARA&A*, 44, 507
- Woosley, S. E., & Heger, A. 2006, *ApJ*, 637, 914
- Zhang, W., Woosley, S. E., & MacFadyen, A. I. 2003, *ApJ*, 586, 356
- Zhang, W., Woosley, S. E., & Heger, A. 2004, *ApJ*, 608, 365

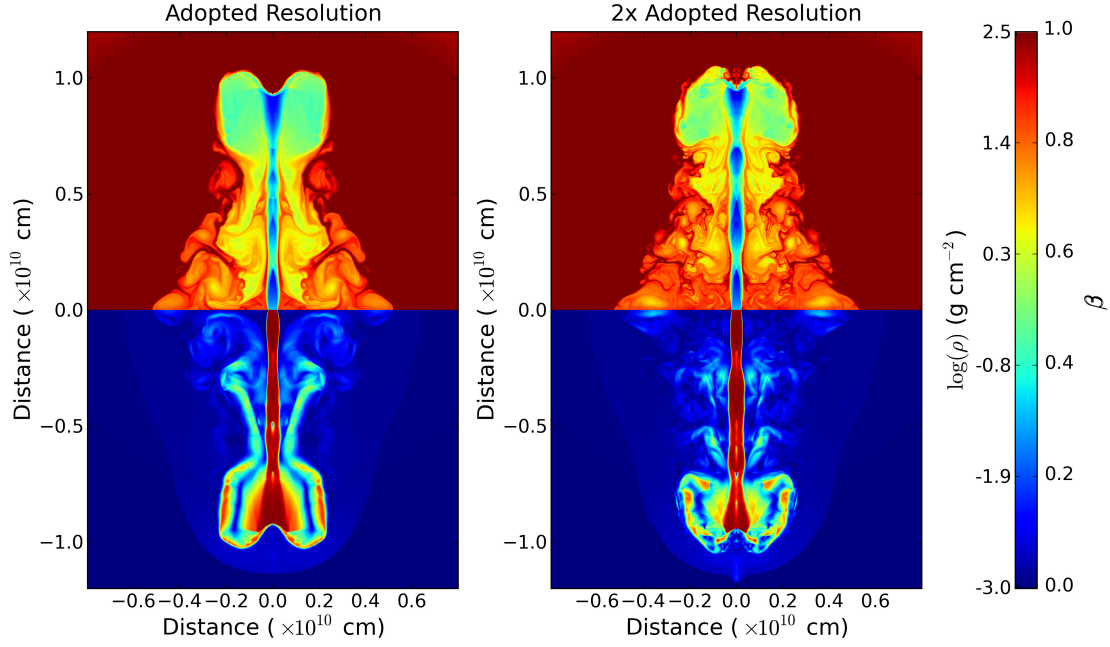


FIG. 1.— Comparison between jets from identical simulations at the adopted resolution (left panel) and at twice the adopted resolution (right panel). The upper part of each panel shows the density map in false colors, while the lower part shows the velocity map. The simulations shown have $t_{\text{eng}} = 10.0$ s and the frames are taken at $t = 6.67$ s after the engine onset. The two jets not only have the same size, but also show the same features, such as a big turbulent eddies on both sides of the head.

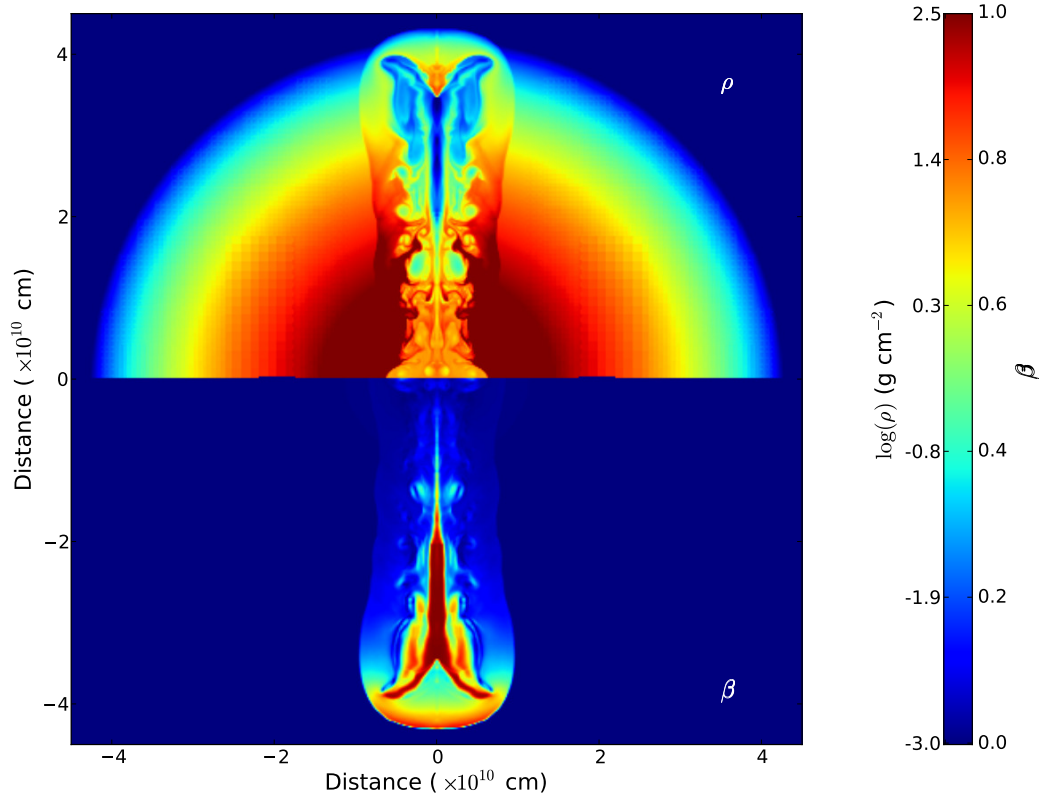


FIG. 2.— Density and velocity maps for the $t_{\text{eng}} = 7.5$ s simulation at breakout ($t = 8.13$ s). The top panel shows a false-color rendering of the logarithm of the density, while the bottom panel shows velocity in units of the speed of light (see color scales on the right).

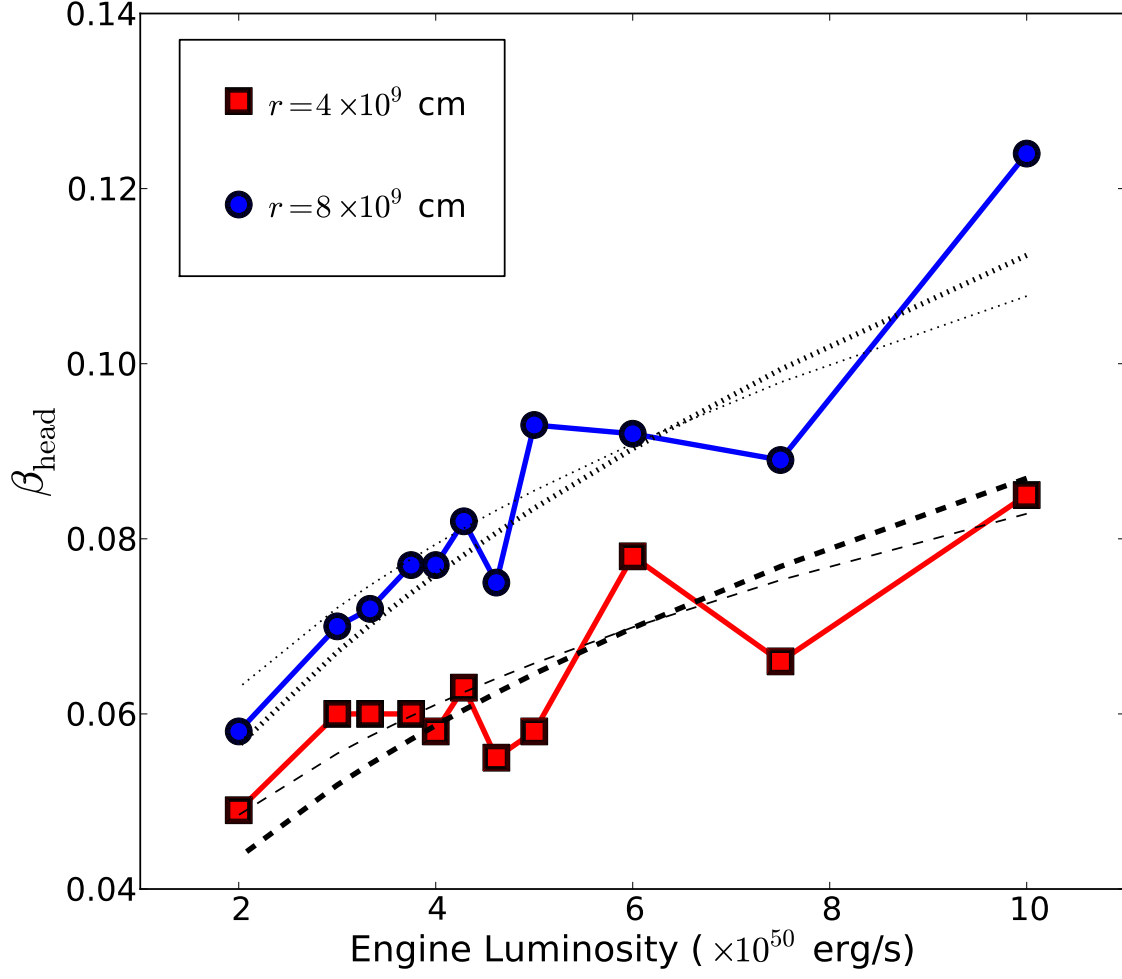


FIG. 3.— Velocity of propagation of the jet head in the stellar material at different stages of the jet-driven explosion. The red curve with squares show the propagation close to the core of the star, as the jet head crosses the distance $r = 4 \times 10^9$ cm. The blue curve with dots show the velocity as the jet head crosses the distance $r = 8 \times 10^9$ cm. Both datasets are obtained from the 16 solar-mass progenitor simulation with total energy $E = 3 \times 10^{51}$ erg. A thick dashed line and a thick dotted line with equation $v_h \propto L_j^{3/7}$ are overlaid on the velocity data for comparison with the analytical prediction of Eq. 6. Thin dashed and dotted lines show instead the comparison with the prediction of Bromberg et al. (2011).

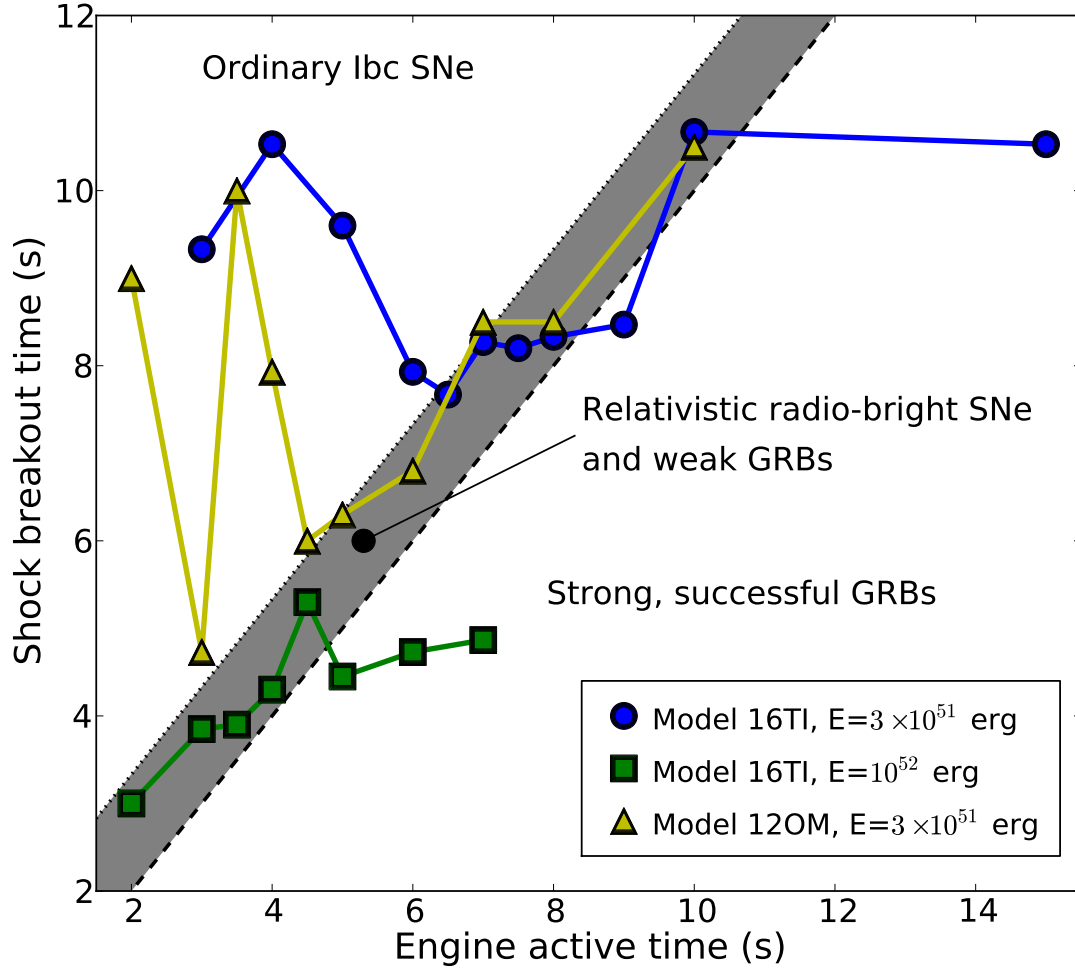


FIG. 4.— Breakout time of the jet/bubble. The black dashed line shows the condition for which the breakout is at the same moment at which the engine turns off. The black dotted line shows the condition for which the breakout takes place after the engine turns off but before the tail of the jet catches up with the jet head.

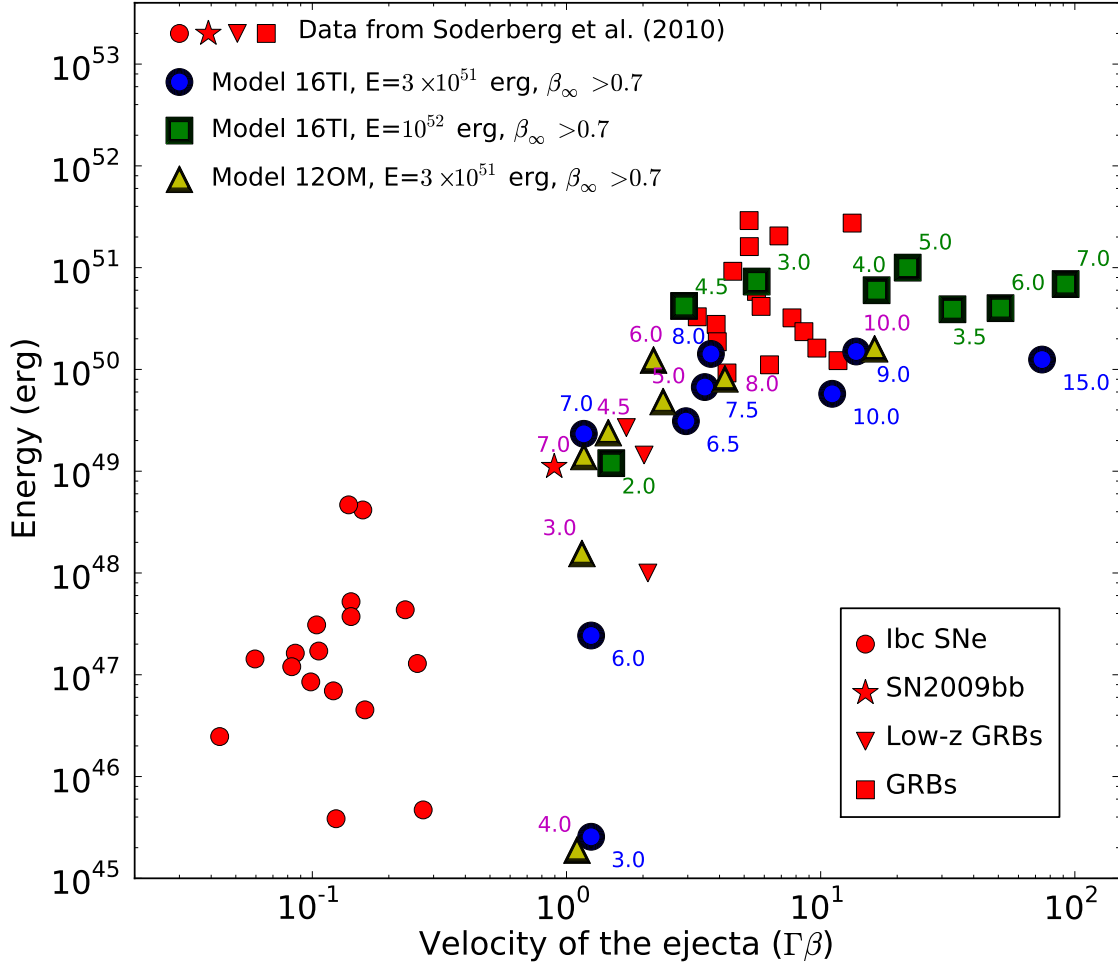


FIG. 5.— Comparison of the simulation results with the observational properties of Type Ibc SNe and jet-driven explosions (red symbols). The results of our simulations are overlaid with blue, green, and yellow symbols (circles, squares, and triangles, respectively) with the duration of the engine activity of each simulation indicated next to each point in the corresponding color.

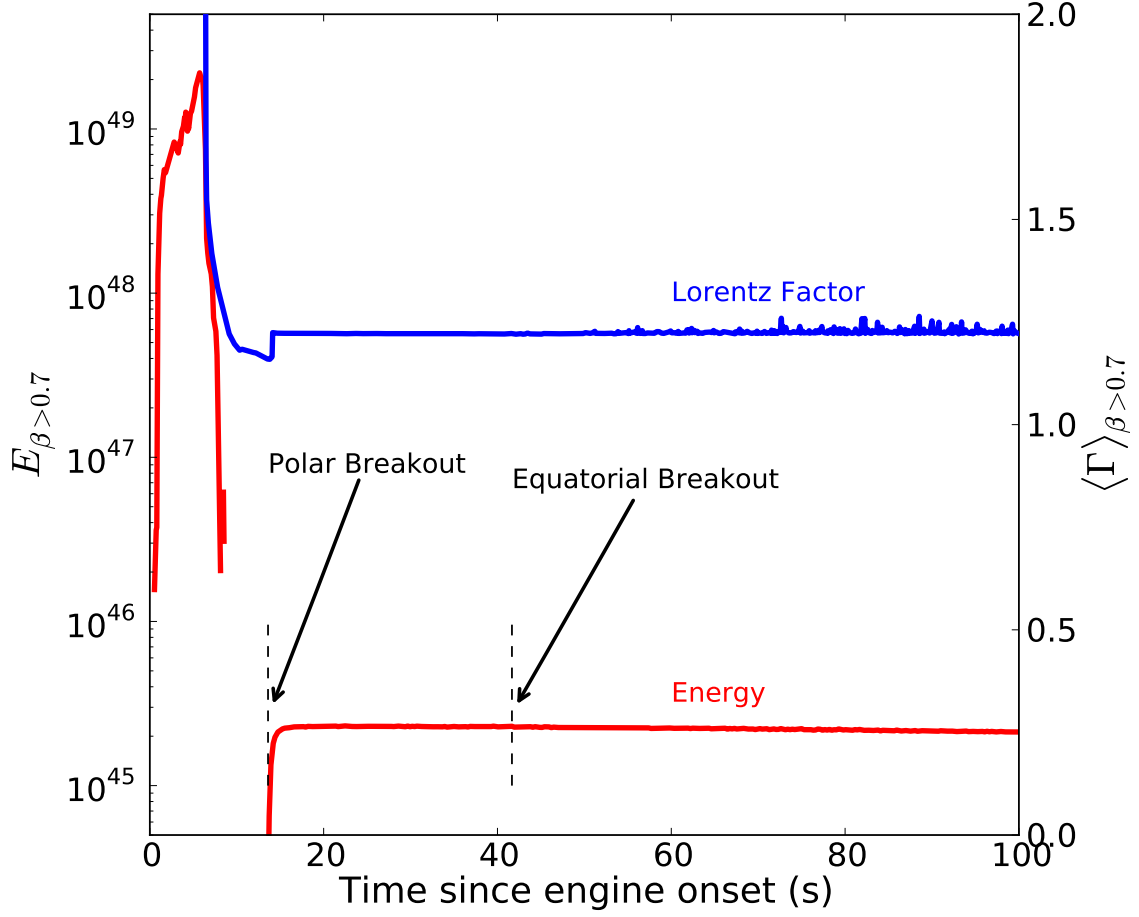


FIG. 6.— Energy in relativistic ejecta (red) and average Lorentz factor (blue) as a function of time after the engine onset for a simulation with $t_{\text{eng}} = 6.0$ s and $E = 10^{51}$ erg. The figure shows that measuring the energy and Lorentz factor just after the shock breakout along the polar axis yield robust results, even if the shock breakout along the equatorial plane has not yet taken place.

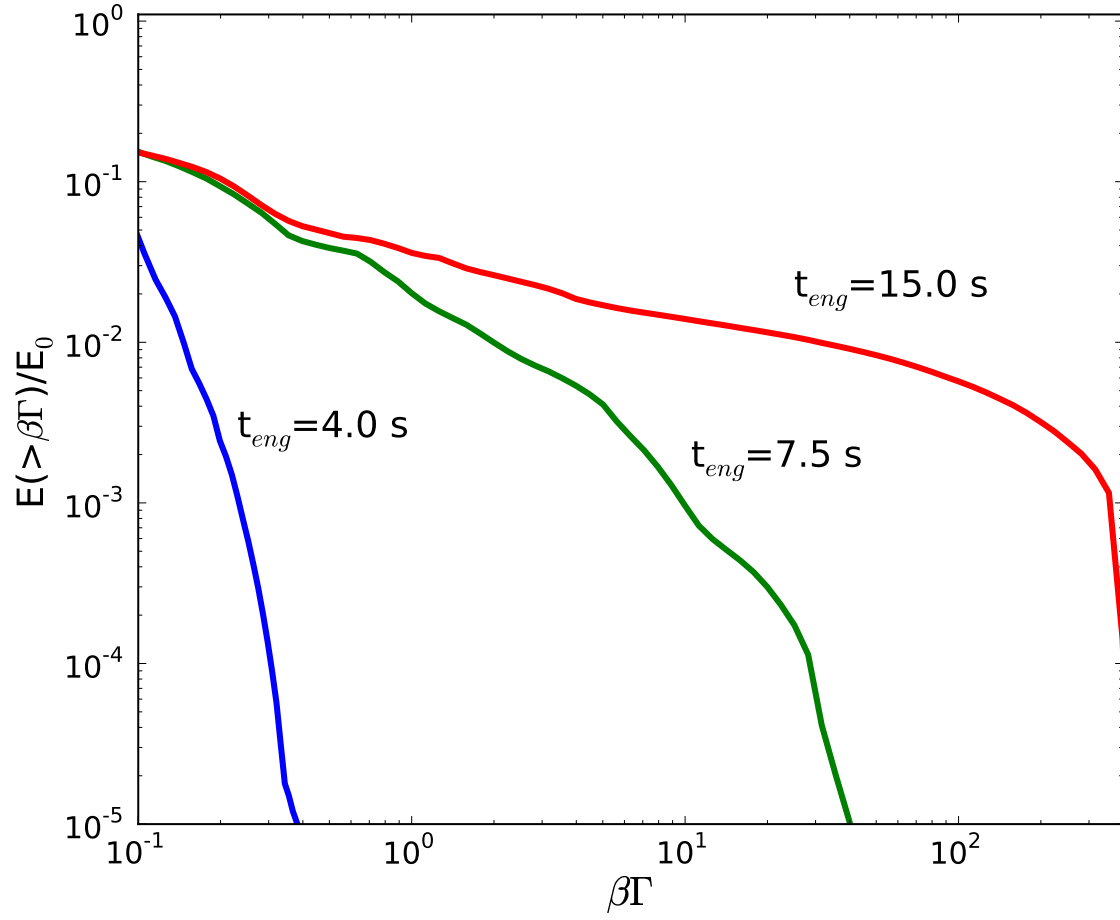


FIG. 7.— Cumulative energy distribution of three representative cases of relativistic jet-driven SN explosions. Simulations resulting in a ordinary SN (blue line), a relativistic SN/weak GRB (green line) and a full-fledged GRB (red line) are shown. All the three simulations have progenitor 16TI and total engine energy $E = 3 \times 10^{51}$ erg.